POLITECNICO DI TORINO
Repository ISTITUZIONALE

Non-Destructive methodology for the evaluation of residual stresses by using Active Infrared Thermography measurements

Original
Non-Destructive methodology for the evaluation of residual stresses by using Active Infrared Thermography measurements / Corsaro, L., Cura, F.M., Sesana, R.. - In: NDT & E INTERNATIONAL. - ISSN 0963-8695. - ELETTRONICO. - 155:(2025), pp. 1-12. [10.1016/j.ndteint.2025.103435]

Availability:
This version is available at: 11583/3000289 since: 2025-05-19T15:38:14Z

Publisher:
Elsevier

Published
DOI:10.1016/j.ndteint.2025.103435

Terms of use:

This article is made available under terms and conditions as specified in the corresponding bibliographic description in the repository

Publisher copyright

(Article begins on next page)

18 November 2026

NDT&E International 155 (2025) 103435

Contents lists available at ScienceDirect

NDT and E International

journal homepage: www.elsevier.com/locate/ndteint

Non-Destructive methodology for the evaluation of residual stresses by using Active Infrared Thermography measurements

Luca Corsaro *, Francesca Curà, Raffaella Sesana

Department of Mechanical and Aerospace Engineering, Politecnico di Torino, C.so Duca degli Abruzzi 24, 10129, Torino, Italy

ARTICLE INFO

Keywords:
Active Infrared Thermography
Lock-in technique
Residual stress
Surface treatments
Thermal diffusivity

ABSTRACT

In this work, a Non-Destructive approach based on an Active Infrared Thermography model is proposed for the evaluation of residual stresses produced by surface treatments. In particular, the thermal diffusivity was chosen as a Non-Destructive thermal index of the investigated surface treatments, and it was carefully evaluated by using Lock-In Thermography measurements. The Active Infrared Thermography model was developed using a similarity to coatings concept that exploits the idea of equivalent thermal diffusivity. In addition, the most relevant factors involved during the Non-Destructive analyses were taken into consideration by means of an Analysis of Variance. The experimental activities were conducted following a complete Design Of Experiment approach composed of both Taguchi Design and Response Surface Methodologies, allowing for the laser parameters calibration with the aim of identifying the interaction between microstructures, residual stresses and thermal diffusivity. This approach resulted in a novel Non-Destructive methodology for the evaluation of residual stresses based on Lock-In Thermography and hardness measurement. The obtained results were compared with the measurements provided by using the X-Ray diffraction meter, allowing errors on the residual stresses evaluation less than 5 %. The validity of the proposed Non-Destructive approach was presented for cylindrical samples and gears with different geometries. Moreover, different surface treatments were also investigated in this work, the induction hardening and the carburizing surface treatments respectively.

1. Introduction

The selection of appropriate surface treatments is of significant importance for ensuring the mechanical resistance of components during operating conditions. This evaluation constitutes a crucial aspect from the preliminary design phase of the component itself. Nevertheless, it is essential that mechanical features, such as hardness and residual stresses, pass a rigorous inspection process before components are put into service.

In general, the inspection of residual stresses is typically realized by employing Destructive, Semi-Destructive and Non-Destructive analysis [1,2]. Non-invasive controls, when combined with green approaches, are now widely preferred due to environmental reasons, and the advantages of Non-Destructive Testing (NDT) techniques largely meet these demands [3,4]. As a matter of fact, the evaluation of residual stresses through NDT techniques, for instance X-Ray or neutron diffractions, magnetic and ultrasonic techniques, can guarantee the integrity of components in many cases. Focusing the attention to the first approach, diffraction techniques exploit crystal structures for residual stress analysis through the use of diffraction signals obtained from the microstructure under investigation. These approaches permit a high level of versatility in terms of their application to different types of components under examination. For instance, as discussed in Refs. [5,6], they can be used to measure the stress of different types of pipes or turbine blades, respectively. Diffraction techniques may, however, be Destructive in certain instances, depending on the geometry of the component. One example of this consideration can be found in the context of complex geometries, such as gears, where the method necessitates the removal of the tooth before the use of diffractometric approaches [7,8]. Alternatively, a number of studies proposed the application of the magnetic method for Non-Destructive detection, specifically the Barkhausen Noise Method (BNM). This technique can also be used for residual stresses evaluation since the detection is performed on the basis of a magnetic-elastic interaction in the magnetic domain [2]. There are many relevant studies on this technique, from residual stresses analysis of samples [9] to mechanical components like aeronautical bearings [10]. A portable device was also developed for the *in-situ* analysis of rail wastes [11]. Recent applications of the BNM

* Corresponding author.
E-mail address: luca.corsaro@polito.it (L. Corsaro).

https://doi.org/10.1016/j.ndteint.2025.103435
Received 10 March 2025; Received in revised form 22 April 2025; Accepted 12 May 2025
Available online 15 May 2025
0963-8695/© 2025 The Authors. Published by Elsevier Ltd. This is an open access article under the CC BY-NC-ND license (http://creativecommons.org/licenses/by-nc-nd/4.0/).

showed a continuous improvement of the current methodology to extend its applications to other research topics. For instance, the feasibility of using this NDT technique to detect the presence of martensite on the surface of rail sections was discussed in Ref. [12] thanks to the use of the envelope of the signals. Furthermore, a primary application of the BNM for the analysis of prestressed strands was carried out in Ref. [13], thanks to the use of a specific solenoid sensor and a dedicated data processing. Acoustic emission is another NDT technique that was extensively discussed in literature. This technique requires particular attention during measurement phases, since coupling conditions may affect the accuracy of results. In the specific case of stresses detection, the interaction between residual stresses and velocity of elastic waves in solid materials is the basis of the analysis [14,15]. Furthermore, it can be adopted for measuring residual stresses also in a combination with a magneto technique, as proposed in Ref. [16].

In the general context of NDT techniques, recent articles were published proposing innovative methodologies for the specific topic of residual stress analysis. The feasibility of the indentation technique was investigated in a number of applications, and the results were promising. In Ref. [17], for example, the problem of non-uniform residual stresses caused by manufacturing and sharpening was discussed, and the problem was investigated in a Non-Destructive manner using the Knoop indentation technique, developing a biaxial residual stress testing method. The integration of the indentation technique with Artificial Intelligence solutions was described in Ref. [18]. More in detail, the residual stress was analysed through the integration of indentation testing technology with Machine Learning (ML) methodologies, allowing the analysis independent of any knowledge of the mechanical properties of metallic materials. The utilization of the eddy current technique as a NDT technique was proposed for the analysis of metal Additive Manufacturing (AM) processes in Ref. [19] on the basis of the temperature-dependent electrical conductivity relation. The authors proposed a method for an *in-situ* temperature monitoring during the AM processes and showed that the induced currents can reflect the temperature changes in steel structures. Consequently, the temperature history could provide an indication of the quality of the material, such as internal stresses, which are otherwise inaccessible for the analysis. The advantages provided by the thermal-electrical relationship was also discussed in Ref. [20]. The authors proposed the investigation of the thermoelectric power (TEP) measurement as a Non-Destructive analysis for the evaluation of microstructural features in the case of a martensitic stainless steel. The obtained results identified that variations in the TEP can be related to the gradual microstructural modifications produced by the heat treatment, resulting in an alternative analysis with respect to the classical approach in which Scanning Electron Microscopy (SEM), X-Ray diffraction and hardness measurements are adopted. In the context of literature on the subject of residual stresses, a novel approach was discussed with regard to the TeraHertz (THz) technique. This technique allows the analysis of the internal information of materials due to its ability to penetrate inside them. Ref. [21] reported the application of THz for a full-field stress measurement method, and a theoretical model based on the stress-optical law was presented, validating the method experimentally for a loaded disk. A further example is proposed in Ref. [22] for Glass Fibre Reinforced Polymer (GFRP). The authors developed a theoretical model based on the anisotropic stress-optics law to describe the THz-elasticity and to calibrate the stress-optic coefficients of GFRP. The proposed approach revealed the relationship between residual stress and the refractive index of GFRP, verifying the feasibility of this technique in measuring residual stress in GFRP.

The field of Infrared Thermography (IRT) is of particular interest as it is a non-invasive method of analysis based on heat emission measured by infrared cameras [23]. Nowadays, a promising application of IRT is the innovative active or stimulated configuration, also known as Active Infrared Thermography (AIRT). In this configuration, samples are thermally excited by an external heating source (laser, induction, lamps, etc.) and the resulting thermal responses are captured by the infrared camera. The first applications analysed composite materials, with many papers describing methods and algorithms to improve defect visibility [24–26]. Subsequently, applications to metallic materials were also explored for topics such as crack detection [27,28], coating analysis [29,30] or damage and material characterization [31,32]. Furthermore, a preliminary application for the anticorrelation analysis between hardness and thermal diffusivity was proposed in Ref. [33], as an alternative to the classical approaches that adopt the photothermal radiometry technique [34–39]. Another recent application of the photothermal technique was presented in Ref. [40], where the combination of advantages provided by photothermal tomography and pulsed thermography resulted in the proposal of a technique named frequency multiplexed photothermal correlation tomography (FM-PCT). The FM-PCT was proposed for Non-Destructive and contactless cross-sectional imaging of manufactured material evaluation and characterization, allowing for three-dimensional thermal images with the aim of evaluating the position of defects or discontinuities in the solid and for rapid detection speed. The potential applications of IRT in the field of stress analysis were also reviewed in the existing literature. For instance, an innovative force-temperature model was properly developed in case of Carbon Fibre Reinforced Polymer (CFRP), as reported in Ref. [41]. The analysis was conducted on the basis of the elastic plate theory and thermal stress analysis, allowing for a novel internal stress measurement technique and composite mechanical behaviour analysis by investigating the temperature distribution on the external surface of the material. In other research works, a combination of both IR and THz techniques was employed for the analysis of residual stress. For instance, in Refs. [42,43], the analysis was conducted for high-density polyethylene (HDPE) material under tensile loading. The Line-Scan Thermography (LST) method was utilized for the quantification of residual stress, adopting the thermal diffusivity as a quantitative detection coefficient. In addition, a comprehensive analysis of the residual stress measurement was conducted using the THz method, which took into account the influence of the refractive index and the sample thickness.

This work proposes an alternative AIRT based Non-Destructive approach for evaluating residual stresses produced by surface treatments. The evaluation is performed by considering Non-Destructive parameters, with a particular focus on thermal diffusivity selected as the AIRT. The analysis was conducted using an AIRT model that was developed on the basis of the most relevant factors involved during the analysis. The overall AIRT activities were conducted according to a Design Of Experiment methodology. Then, a range of case studies were considered to validate the proposed Non-Destructive approach. At the end, a comparison of the estimated results with those obtained from the X-Ray diffraction meter indicated errors of less than 5 % in the residual stresses evaluation.

2. Mathematical formulations

2.1. Thermal diffusivity estimation by means of the "Slope Method": analytical background

The assessment of thermal properties requires the measurement of the thermal conductivity (k), that can be determined using a conventional apparatus such as the Hot Disk instrument. In order to obtain accurate results, it is essential that the samples under analysis are manufactured in accordance with the specific requirements of the apparatus or Standards. Then, the thermal diffusivity (α) can be calculated through a computation with the specific heat and the density.

The capability to estimate α remains a topic of significant interest within the Thermographic field. As a matter of fact, a variety of AIRT configurations can be employed, depending on the AIRT technique (either the Lock-In or the Pulsed technique) and the experimental setup (either a reflection or a transmission configuration). In some cases, particular attention must be paid to the geometry of the sample, as with

the applications of the ISO 18555 and 18755 Standards [44,45]. On the other hand, the "Slope method" appears to be less sensitive to the sample geometry of the samples, allowing for a localised estimation of α for all sample geometries.

In this study, α was selected as a thermal index for the objective of evaluating residual stresses produced by surface treatments. The calculation was performed in accordance with the isotropic analytical formulation for slabs proposed in Ref. [46], as summarized below.

Let us consider a specific case in which the heating source is a laser beam of power P_0, modulated with a certain frequency f and with a radius equals to a. In the context of a slab geometry (see Fig. 1) of thickness l, the periodic thermal response in terms of temperature can be defined in a generic formulation using the Hankel space with cylindrical coordinates:

$$T_{(r,z)} = \int_0^\infty \delta J_0(\delta r)\left[A\, exp^{\beta z} + B\, exp^{-\beta z}\right] d\delta \tag{1}$$

where δ is the Hankel variable, J_0 is the Bessel function, β is the thermal wave vector and A and B represent specific constant tuned on the basis of the boundary conditions and heat flux continuity.

When considering a small temperature rise and a Gaussian distribution of the laser beam as $\left(P_0/\pi a^2\right)exp^{-2r^2/a^2}$, two possibles cases can be defined on the basis of the thickness l and the thermal diffusion length (μ) parameter [46] introduced in equation (2).

$$\mu = \sqrt{\frac{\alpha}{\pi f}} \tag{2}$$

In the first case, a "thermally thin" slab is considered. The thickness of the slab is less than the thermal diffusion length ($l \ll \mu$) and equation (1) can be rearranged as:

$$T_{(r)} = P_0 \Big/ 4\pi Kl \int_0^\infty \delta J_0(\delta r)\left(exp^{-(\delta a)^2/8}\right) \Big/ \beta'^2 d\delta \tag{3}$$

where $\beta'^2 = \delta^2 + \sigma'^2$ and $\sigma'^2 = \sigma^2 + (2h/kl)$, where k is the thermal conductivity and h the heat transfer coefficient of the slab surfaces. In the particular case of a laser beam radius equals to zero ($a = 0$), and for distances that are significantly larger than the beam width ($r \to \infty$), an analytical solution to equation (3) can be derived. In particular, the thermal wave propagates in a cylindrical manner along the radial direction according to the following equation:

$$T_{(r\to\infty, a=0)} \approx P_0 \Big/ 4\pi Kl\sqrt{\pi/2}\left(1 \Big/ \sqrt{\sigma'_R + i\sigma'_I}\right)\left(exp^{-\sigma'_R r}/\sqrt{r}\right) exp^{-i\sigma'_I r} \tag{4}$$

where σ'_R and σ'_I correspond to the real and the imaginary part of σ'. Equation (4) allowed to point out the following considerations. The phase signal of the temperature response shows a linear behaviour with respect to the r dimension, which slope is equal to σ'_I. On the other hand, the natural logarithmic of the amplitude signal of the temperature response exhibits a linear response in relation to the $\sqrt{r}$, which slope corresponds to σ'_R. A more realistic scenario involves a real radius dimension of the laser excitation source. In this scenario, the observed linear behaviour is confirmed for large r dimensions.

The second case is the "thermally thin" slab ($l \gg \mu$). Equation (1) can be rearranged as:

$$T_{(r,z=0)} = P_0 \Big/ 4\pi K \int_0^\infty \delta J_0(\delta r)\left(exp^{-(\delta a)^2/8}\right) \Big/ (\beta + h_0/K)\, d\delta \tag{5}$$

but, in this case, no analytical solutions were available. In any case, the validity of the proposed formulations for the α estimation was validated by the authors [46] through numerical simulations. In the specific case of phase signal as thermal response, as implemented in this study, the estimation of α can be derived as follows:

$$m = \sqrt{\frac{\pi f}{\alpha}} \tag{6}$$

where the slope of the phase signal is defined with m.

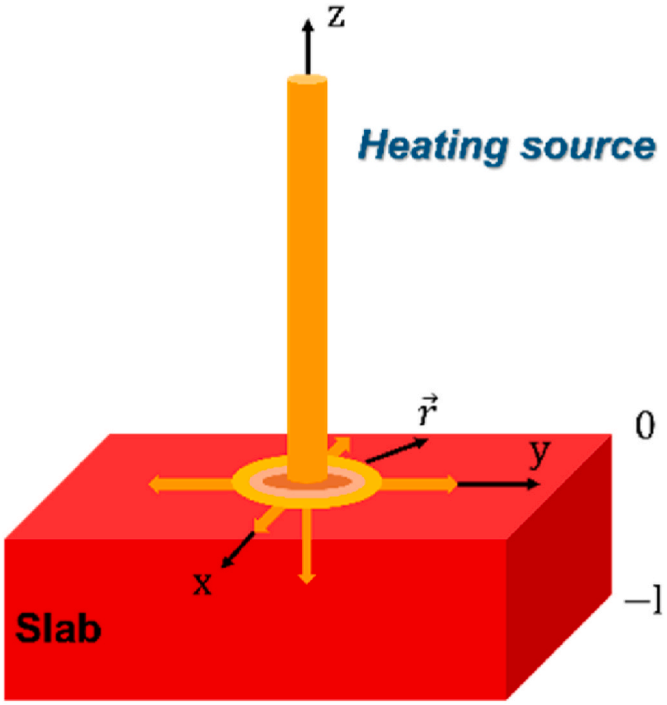


Fig. 1. Slab geometry.

2.2. AIRT model for the residual stresses evaluation

The proposed AIRT model provides a non-invasive evaluation of the superficial residual stress entity exploiting both mechanical and thermal properties. Regarding the thermal properties, α was evaluated by using AIRT measurements according to the "Slope Method" as presented in Section 2.1, becoming a thermal index representative of the material under investigation.

As described in Section 1, the anticorrelation phenomena between hardness and α was widely discussed through the use of photothermal radiometry technique [34–39]. More in detail, the local value of α was compared to the corresponding local hardness, and the analysis was performed along the depth of the material by using an inversion methodology. In these studies, the photothermal formulation was adopted and inversion algorithms were necessary to obtain α. On the contrary, there is a lack of discussion in literature on the possible relation between the residual stress state and α.

The idea of the proposed AIRT model is based on the analysis of the surface treatment as a coating that affects both mechanical and thermal properties at a superficial layer. Fig. 2 (a) shows a scheme of the surface treatment effect on both mechanical and thermal properties. In particular, the red colour denotes to the untreated material (material without surface treatment, UTM), while the green colours refer to the treated material (material with surface treatment, TM). In case of surface treatments such as induction hardening and carburizing, the positive effects observed on both hardness and compressive residual stress properties are attributed to microstructural changes. This microstructural modification also affects the thermal properties with a consequent impact on the heat propagation along the depth of the material. On the basis of these considerations, it can be concluded that the mechanical and thermal properties of the untreated material are uniform along the depth. On the contrary, in case of material subjected to surface treatment, these properties may differ from the surface to the substrate zone

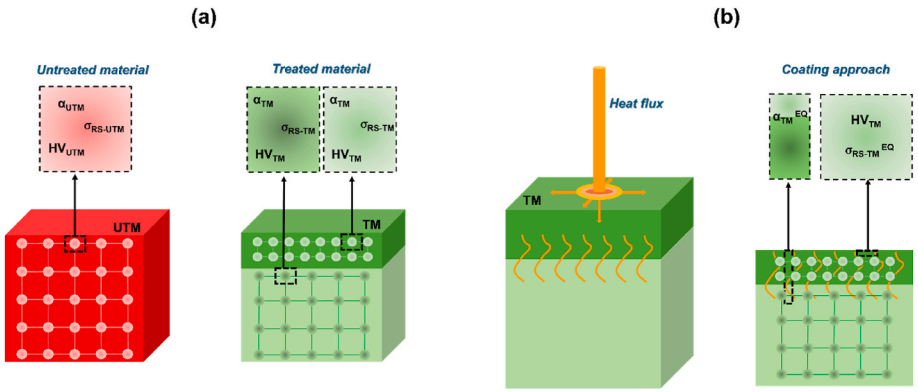


Fig. 2. Surface treatment analysis: (a) material properties, (b) Similarity with the coating.

which may or may not be considered very close to the untreated material, depending on the surface treatment. So, the superficial hardness is defined as a local mechanical property derived from the local superficial microstructure. On the other hand, the compressive residual stress distribution is generated by the interaction of different microstructures (with different densities) along the material depth, as a consequence of the treatment itself. Regarding thermal properties, it is possible to obtain different values of α depending on the microstructure.

Fig. 2 (b) provides a schematic representation of the coating approach adopted for the AIRT model. The phenomenon of the heat propagation that occurs during AIRT tests involves the material in its thickness, and, in the specific case of the treated material, several microstructures are intercepted by the heat flux. It can be concluded that an equivalent thermal diffusivity value for the treated material ($\alpha_{TM}{}^{EQ}$) can be considered, based on the microstructures at both surface (the coating part) and depth (the substrate part). This approach is the same in case of coatings [44], where an equivalent microstructure can be considered for the purpose of an equivalent thermal characterization. In a similar manner, the concept of these equivalent microstructures can also be explored in relation to the mechanical properties.

In this study, an equivalent value of superficial residual stresses, which could also be adopted specifically for each surface treatment, was considered as the results of the interaction of the whole microstructure along the depth and the volume of the material. So, the idea of a mean value of the surface residual stresses measured along two perpendicular directions was used as an indicator of the overall microstructural change. Regarding the hardness, the same superficial zone tested with AIRT was considered for the analysis.

From a mathematical point of view, the following formulations were proposed for the specific purpose of developing a Non-Destructive approach. Let now consider both thermal and hardness properties, that can be obtained in a Non-Destructive manner. The behaviour defined for each material condition (treated and untreated materials respectively) from Non-Destructive experimental measurements was mathematically described choosing a linear modelling of the anti-correlation phenomena:

$$H = p\alpha + d \tag{7}$$

in particular, H corresponds to the hardness in Vickers value, p is the slope and d is the intercept. It's important to note that α proposed in equation (7) may represent the thermal diffusivity or the equivalent thermal diffusivity, on the basis of the tested material, indicating a general thermal index properly estimated through AIRT measurements. For the final purpose of Non-Destructive residual stresses evaluation, a proposal of a logarithmic formulation was considered by using the following mathematical description:

$$\sigma_{RS} = \frac{1}{n}\ln\left(\frac{H_{TM}}{H_{UTM}}\right) \tag{8}$$

where σ_{RS} corresponds to the superficial compressive residual stress, n is defined as the AIRT coefficient, H_{TM} is the hardness in Vickers measurements of the treated material and H_{UTM} is the hardness in Vickers measurements of the untreated material. The n coefficient was properly defined with the idea of utilizing Non-Destructive measurements previously introduced in equation (7). For this aim, an analysis of the relevant factors involved during AIRT tests was also carried out by means of a statistical analysis, an Analysis of Variance (ANOVA) respectively. A formulation for the n coefficient (n^*) based only on factors influencing the AIRT measurements was then developed, taking into account the specific effect of the microstructural change produced by the surface treatment. The mathematical formulation is proposed in following equation.

$$n^* = \frac{1}{ST^*|p|} \tag{9}$$

Then, the ST coefficient proposed in equation (9) was properly investigated on the basis of the surface treatment, allowing an error in the estimation of σ_{RS} less than 5 %. The optimal results were obtained with a ST coefficient equal to 2.7 for the carburizing surface treatment, while a value of 2.4 was used for the induction hardening surface treatment. The model calibration is described in the result section.

The validity of the proposed AIRT model concerns surface treatments in which the microstructural change has a significant effect on heat propagation compared to the untreated material behaviour. This way, the results of a Non-Destructive analysis (thermal index, α, and superficial hardness, H, measurements) can be adopted for evaluating the σ_{RS} entity.

3. Materials and methods

3.1. Specimens

This study proposes the estimation of residual stresses for cylindrical samples and gears subjected to two different surface treatments, an induction hardening surface treatment (for the C45 steel) and a carburizing surface treatment (for the 20MnCr5 steel), respectively. Moreover, a set of two different gear geometries, in terms of different modulus, were also investigated.

The case studies considered in this activity are summarized in Table 1, while Fig. 3 illustrates, as an example, the possible specimen geometries. It is important to emphasise that untreated and treated gears (for each case study) show the same surface appearance, and the only difference is the presence of the surface treatment which is imperceptible from a visual point of view.

Referring to Table 1, the columns report the specimen type (first column: cylindrical samples, 3 mm modulus gears and 4 mm modulus gears), the tested materials (second column: 20MnCr5 and C45 steels),

Table 1
Specimens and surface treatments: case studies.

Specimen type	Material	Geometry	Tested conditions
Cylindrical samples	20MnCr5 steel	-Cylindrical shape -Thickness: 10 mm -Diameter: 45 mm	-Untreated material -Carburized material
Cylindrical samples	C45 steel	-Cylindrical shape -Thickness: 10 mm -Diameter: 45 mm	-Untreated material -Induction hardened material
3 mm modulus gears	20MnCr5 steel	-Spur gear -N° of teeth: 20 -Pressure angle: 20° -Gear width: 28 mm	-Untreated material -Carburized material
4 mm modulus gears	20MnCr5 steel	-Spur gear -N° of teeth: 20 -Pressure angle: 20° -Gear width: 40 mm	-Untreated material -Carburized material
3 mm modulus gears	C45 steel	-Spur gear -N° of teeth: 20 -Pressure angle: 20° -Gear width: 28 mm	-Untreated material -Induction hardened material

the specimen geometries (third column: cylindrical shape or spur gears) and the tested conditions (fourth column: untreated, induction hardened and carburized materials). So, a total number of 10 specimens (4 cylindrical samples and 6 gears), untreated and treated, were utilized in this study. A high level of production quality was required from the manufacturer in terms of material properties and surface treatment uniformity of all specimen typologies (cylindrical samples and gears, treated and untreated materials). Moreover, the untreated and treated specimens were manufactured from the same steel bars in order to reduce as much as possible the variability in the chemical composition of the steel, which could affect the mechanical and thermal properties, so that the variability in the measured results was limited to the microstructural changes caused by the surface treatment.

A detailed mechanical properties analysis was firstly investigated with a classical apparatus. The residual stresses of cylindrical samples were measured along two perpendicular directions with an X-Ray diffraction meter, while the hardness was evaluated at a series of points on the planar surface. For what concerns gears, the residual stress analysis was conducted by using an X-Ray diffraction meter in both radial and longitudinal directions after the tooth was extracted from the gear. The values were obtained at the centre of the tooth and close to the pitch diameter, that represents a zone of interest in ISO Standards computations [47]. Metallographic analyses were also conducted in order to investigate the microstructure and the hardening pattern of the tested gears. The micro hardness values were evaluated on the tip of the tested tooth and along the depth of the hardening pattern (in the proximity of the pitch diameter) by using a micro-durometer.

The X-Ray diffraction meter utilized in this activity exhibited a Theta-Theta geometry, equipped with a Cr anode (30 kV and 0.1 mA) and a linear silicon strip detector based on single photon counting technology. The hardness values for all the investigated specimens (cylindrical samples and gears) were evaluated by using the Vicker method with a load of 0.1 kg. The choice was motivated by the fact that the Vicker hardness is generally used to define the resistance of gears in the ISO Standard [48].

3.2. Active Infrared Thermography setup

The AIRT setup was already utilized as Non-Destructive approach for the local residual stress identification on both samples and gears [49]. Fig. 4 illustrates the experimental setup adopted for both cylindrical samples and gears (as an example for the 4 mm modulus geometry).

The equipment was composed of a thermal camera FLIR A6751sc (sensitivity lower than 20 mK and 3–5 μm spectral range), a laser excitation source (that can generate a square wave as heating profile, 50 % of duty cycle, a maximum power of 50 W concentrated in a small surface) and a PC control unit. In case of gears, a special F-Theta optical lens was utilized to reduce and to localize the heating over the tip of the tooth. The thermal camera and the heating source were placed in front of the specimens (samples or gears), implementing the so-called "reflection mode" configuration during the AIRT tests.

3.3. Laser parameters calibration: a Design Of Experiment approach

The Lock-In technique was identified as the optimal AIRT technique for surface treatments identification when thick samples or components such as gears are involved [49–51]. In general, a laser heating source is controlled acting on three parameters: the power, the step duration and the number of cycles. In order to realize the Lock-In technique, all parameters are involved during the heating phase and, for this purpose, the optimal laser parameters combination was accurately evaluated by following a Design Of Experiment (DOE) approach.

The laser parameters were evaluated for the untreated material. This assumption was motivated by the fact that untreated materials are characterized with a very low value of residual stress for definition, and the thermal properties are also easy to thermally characterize since they are generally constant along the depth of the material. Moreover, the laser parameters were evaluated for each case study (see Table 1). This way, the adopted approach enabled the compensation of the potential impact of different geometries and experimental setups (the presence or absence of the F-Theta lens) on the heat propagation, and consequently on the estimation of a possible thermal index.

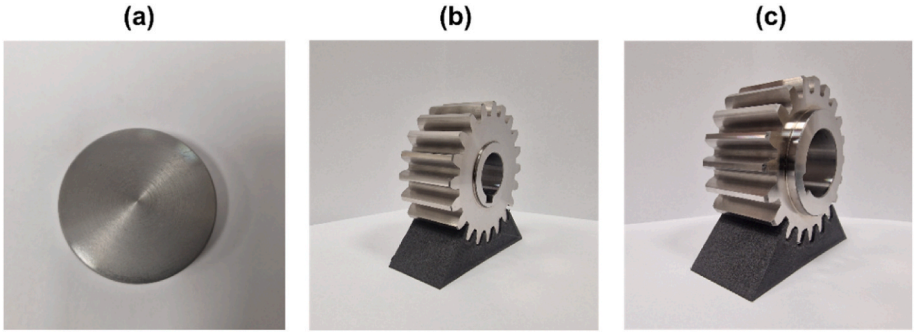


Fig. 3. Specimen geometries: (a) cylindrical sample, (b) 3 mm modulus gear, (c) 4 mm modulus gear.

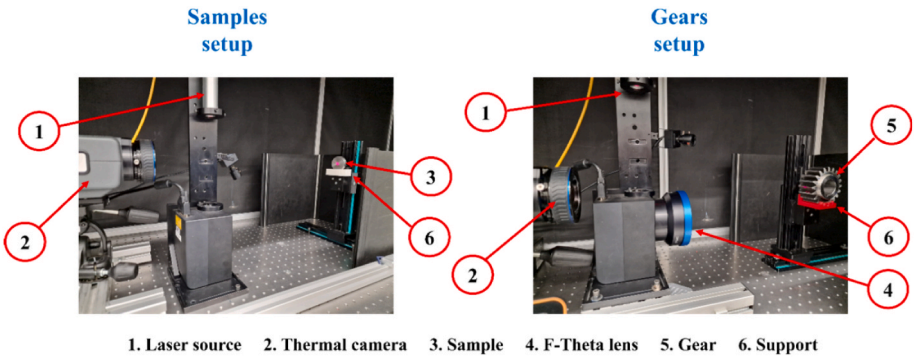


Fig. 4. AIRT setup for cylindrical samples and gears.

Fig. 5 (a) reports the most relevant steps involved during the DOE activity. The initial step (thermal index definition, see Fig. 5 (a)) involved the selection of an appropriate thermal index capable of detecting thermal alteration produced by microstructural changes resulting from surface treatments. Preliminary analyses [50,51], in which Hot-Disk apparatus was employed, indicated that the thermal diffusivity was the most appropriate thermal index for this purpose. In this work, the thermal diffusivity was estimated by using the Slope Method (see the mathematical formulations presented in Section 2), and it was adopted as the response variable during the DOE activity. During the AIRT tests, cylindrical samples and gears were heated with the laser source as illustrated in Fig. 5 (b), and the thermograms were elaborated by using IRTA2 Software. Subsequently, thermal responses (phase signals) were extracted along lines located over the cylindrical sample surface and the tip of the tooth (see Fig. 5 (b)). The tooth tip was chosen for the analysis as it corresponds to a planar surface in front of the thermal camera.

Subsequent to the thermal index definition, the laser parameter tuning was carried out with the second and third steps of the DOE activity (see Fig. 5 (a)). The three laser parameters (power, step duration and number of cycles) were considered as factors, while the target response utilized for the tuning of the laser parameters was α of the C45 and 20MnCr5 untreated steels. These target values were estimated from dedicated thermal conductivity measurements by using the classical Hot-Disk from untreated cylindrical samples [50,51] and, in addition, the tested gears were manufactured from the same cylindrical bars. A preliminary laser parameter combination was identified by employing the Taguchi Design (Preliminary laser parameters combination step, see Fig. 5 (a)) in the "nominal-is-best" condition [52]. An L27 orthogonal array was adopted, with each factor varying with three levels, and each combination repeated three times. This approach facilitated the identification of the most relevant factors by investigating the impact of each factor on the Signal-to-Noise ratio, the mean and the standard deviation of the response. Subsequently, starting from the previous preliminary combination, an optimal laser parameter combination was defined (Optimal laser parameter combination step, see Fig. 5 (a)) by using the Central Composite Design (CCD) as Response Surface Methodology (RSM) [53], and the tested combinations were repeated twice. At the end, the optimal laser parameters were then identified by means of the surface plot.

After identifying the optimal combination of laser parameters, the AIRT setups were validated by performing three AIRT tests for each case study (Laser parameters check step, see Fig. 5 (a)). Then, a mean value of the thermal index was considered to verify the results with respect to the target responses provided by the Hot Disk analysis [50,51]. So, any deviation in the thermal response can be attributed solely to microstructural changes induced by the surface treatment, which can be quantified through the thermal index computation.

4. Results and discussion

Firstly, the results of the mechanical properties characterization (hardness and surface residual stress by using the X-Ray diffraction meter) of all specimens are presented.

The comparison of the investigated mechanical properties for the untreated and treated (carburized and induction hardened materials) cylindrical samples is shown in Fig. 6 ((a) and (b)). In particular, the line refers to the hardness variation, while the grey bars correspond to the X-Ray surface residual stress values. In particular, the x and y grey bars refer to the superficial residual stress measurements obtained along two perpendicular directions (see section 3.1). Similar results are reported for gears (Fig. 6(c) and (d) and (e)). In this case, the graphs show a comparison of the mechanical properties (hardness and X-Ray residual stress) between untreated and treated gears, carburized and induction hardened respectively. In particular, the x grey bars represent the superficial residual stress measurements along the longitudinal direction, while the y grey bars denote the superficial residual stress measurements along the radial direction (see section 3.1). From the analysis of Fig. 6 in all parts, it can be observed that the microstructural change caused by the surface treatments (carburizing and induction hardening processes)

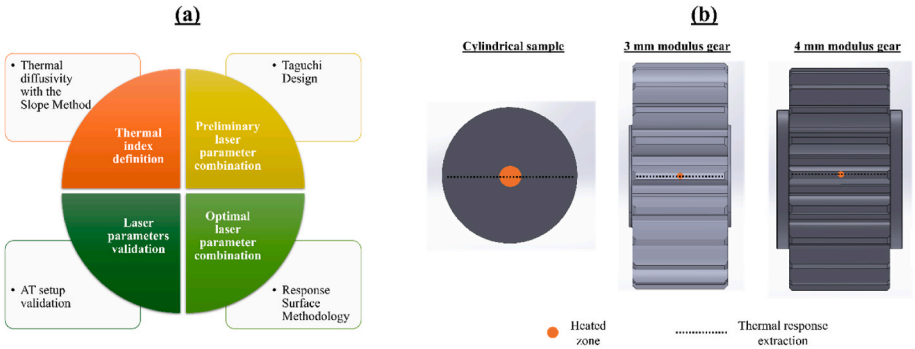


Fig. 5. DOE activity: (a) steps (b) investigated zones.

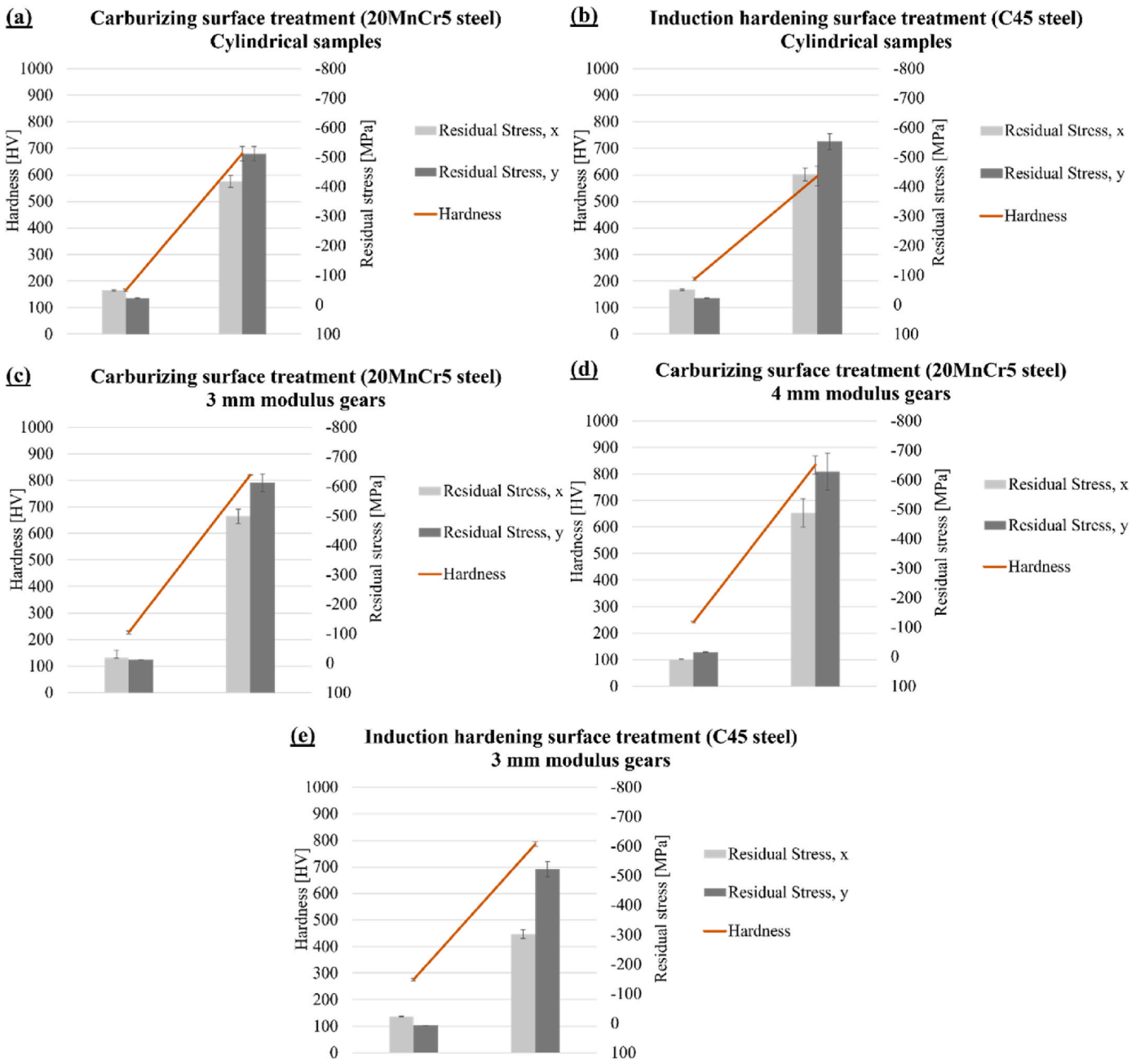


Fig. 6. Mechanical properties characterization: (a) (b) cylindrical samples, (c) (d) (e) gears.

increased the mechanical properties as expected, resulting in an increment of both hardness and surface residual stresses. The same behaviour was observed for both cylindrical samples and gears (3 mm and 4 mm moduli).

Fig. 7 (a) shows the metallographic analysis carried out in case of gears for both surface treatments, while Fig. 7 (b) reports the micro hardness analysis performed along the depth of the tooth. For sake of simplicity, the analysis of the surface treatment pattern for the carburizing surface treatment is proposed for the 4 mm modulus gear. For the induction hardening surface treatment, the microstructural change involved approximately the entire tooth up to the root (Fig. 7 (a), martensitic microstructure - A), while a microstructural transition was observed at the root zone (Fig. 7 (a), mixed microstructure - B). In case of carburizing surface treatment, a martensite microstructure can be identified as an external layer as a result of the carburizing enrichment (Fig. 7 (a), martensite microstructure - C), while the internal part of the tooth exhibited a mixed microstructure as a consequence of the heating and quenching processes (Fig. 7 (a), mixed microstructure - D). Focusing the attention on the micro hardness measurements (see Fig. 7 (b)), the obtained hardening pattern produced a microstructural evolution along the depth characterized by a micro hardness decrement. The induction hardening surface treatment is responsible for a relatively homogeneous microstructure along the depth of the tooth, resulting in a less significant micro hardness variation along the depth, although a slight decrement was observed in the measurements. Moreover, the microstructural change produced by the surface treatments over the teeth was found to be identical in both the tip and pitch diameter zones. This indicates that, in the specific case of gears, even if the microstructural changes were investigated by heating the tip, they can be considered comparable to those evaluated at a point of interest, such as the pitch diameter.

The results obtained during the DOE activity are presented in the following part. Fig. 8 illustrates the surface plots generated from the

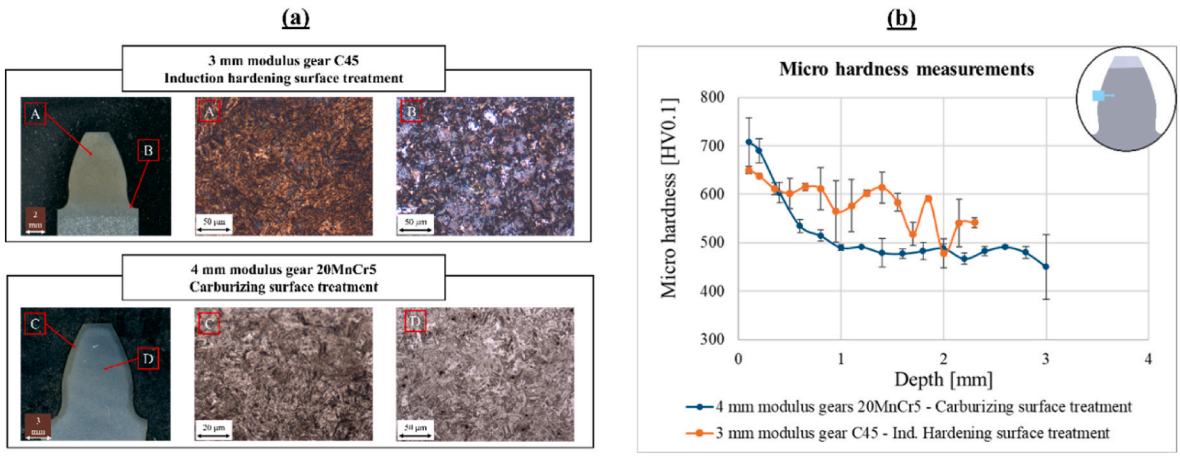


Fig. 7. Surface treatment patterns: (a) metallographic analysis, (b) micro hardness along the depth.

RSM analysis (Optimal laser parameters combination step, see Fig. 5 (a)), specifically for cylindrical samples (Fig. 8 (a)) and 3 mm modulus gears (Fig. 8 (b)), to provide an example during the tuning of the laser parameters.

In the specific case of Fig. 8, the laser parameters evaluation was achieved through the adjustment of two factors (step duration and power of the laser source) that were identified as the most important factors during the Taguchi Design analysis (Preliminary laser parameters combination step, see Fig. 5 (a)). Subsequently, the optimal laser parameters were tuned with the objective of estimating α of the untreated material under investigation. Table 2 shows the results obtained from the DOE activity for all the case studies. More in detail, the optimal laser parameters columns report the optimal combination of step duration, power and number of cycles obtained from the RSM activity. Then, the thermal index column shows the target response (α from the Hot Disk measurements) and the corresponding errors generated with respect to the thermal index estimated by using the AIRT setup. The energy provided during the AIRT tests is also illustrated, and an estimation of the investigated depth (heat penetration) was also calculated for each case study with the thermal diffusion length (see equation (2)). From an analysis of Tables 2 and it can be seen that gears and samples exhibit different laser parameters combinations. This is due to the fact that gears undergoing testing with the F-Theta lens, which necessitates a dedicated tuning of the laser parameters to avoid excessive heating over the tooth surface. It is also important to note that a standardized experimental setup in term of laser parameters was obtained for gears. This result is supported by the observation that the target thermal diffusivity of both C45 and 20MnCr5 steels, in the untreated condition, is very similar. Consequently, it can be concluded that the different gear geometries (3 mm modulus and 4 mm modulus) have a comparable effect on the heat propagation, and the same laser parameters can be used during AIRT tests. On the other hand, the absence of the F-Theta lens produces two distinct combinations of laser parameters for cylindrical samples. Regarding the error with respect to the target response, the 20MnCr5 steel exhibited low error values in the thermal index estimation in comparison to those obtained in case of C45 steel. The optimal laser parameters were then utilized to test both untreated and treated specimens.

The results obtained from both Destructive and Non-Destructive analyses are summarized in Table 3, for both untreated and treated materials, and for each case study. In particular, the Destructive analysis is referred to the experimental activities devoted to the measurement of residual stresses by means of the X-Ray diffraction meter. In case of gears, the investigated tooth was completely removed from the gear, resulting in Destructive measurements due to the complexity of its geometry. The σ_{RS} values detailed in the Destructive analysis column of Table 3 correspond to a mean value of the surface residual stresses presented in Fig. 6, as defined in Section 2.2. The column reports values for both untreated and treated materials and for each case study. In particular, a null value was assigned for the untreated material due to the low value of residual stresses. Conversely, the Non-Destructive analyses are referred to the results obtained from micro hardness and thermal index investigations. The specimens were analysed without destroying the components since local micro hardness measurements were performed from the tip of the tooth, while the thermal index was estimated by using the AIRT measurements proposed in sections 2.1, 3.2

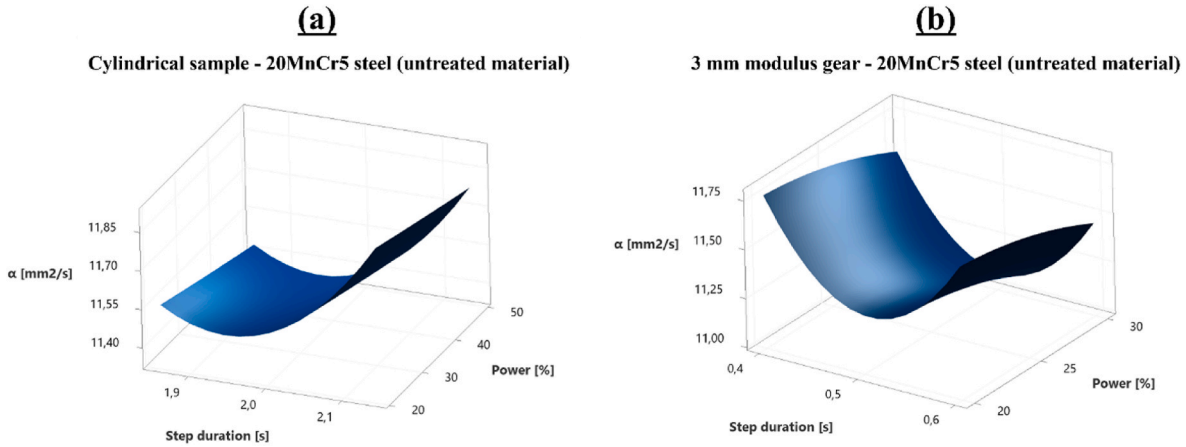


Fig. 8. Surface plots: (a) cylindrical samples - 20MnCr5 steel, (b) 3 mm modulus gear - 20MnCr5 steel.

Table 2
DOE Activity: laser parameters combination.

Case study	*Optimal laser parameters*			*Thermal diffusivity estimation*		*Energy*	*Heat penetration*
	Step duration [s]	Power [W]	N° cycles [−]	Target [mm^2/s]	Error [%]	[J]	[mm]
Cylindrical samples 20MnCr5 untreated steel	1.9	22.5	200	10.59	6.35	8550	2.5
Cylindrical samples C45 untreated steel	1.5	50	120	11.10	11.98	9000	2.5
3 mm modulus gears 20MnCr5 untreated steel	0.5	15	200	10.59	4.56	1500	1.3
4 mm modulus gears 20MnCr5 untreated steel	0.5	15	200	10.59	1.68	1500	1.3
3 mm modulus gears C45 untreated steel	0.5	15	200	11.10	18.92	1500	1.4

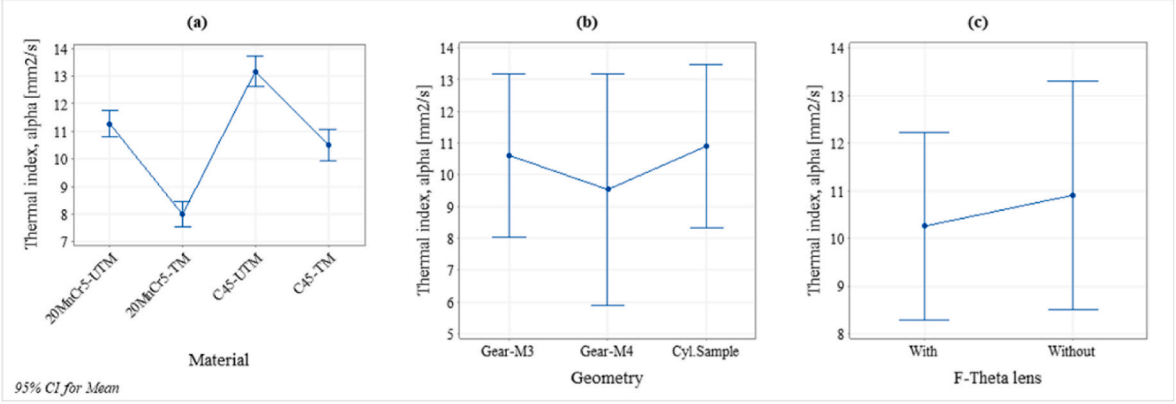
Table 3
Destructive and Non-Destructive analysis: mechanical and thermal results.

	Destructive analysis		Non-Destructive analyses			
Case study	*Compressive residual stress, σ_{RS} [MPa]*		*Micro hardness, H [HV]*		*Thermal index, α [mm^2/s]*	
	Untreated material	Treated material	Untreated material	Treated material	Untreated material	Treated material
Cylindrical samples	0	465	165.17	679.82	11.59	7.99
20MnCr5 - Carburizing surface treatment		±66	±4.53	±27	±0.11	±0.04
Cylindrical samples	0	497	208.06	595.32	13.16	10.90
C45 - Ind. Hardening surface treatment		±78	±5.87	±37.61	±0.22	±0.63
3 mm modulus gears	0	555	220.67	820.67	11.34	7.81
20MnCr5 - Carburizing surface treatment		±81	±2.55	±2.14	±0.06	±0.09
4 mm modulus gears	0	558	262.90	833.45	10.89	7.82
20MnCr5 - Carburizing surface treatment		±99	±11.54	±36.66	±0.09	±0.08
3 mm modulus gears	0	412	298.92	788.10	13.20	10.11
C45 - Ind. Hardening surface treatment		±156	±10.63	±27.21	±0.26	±0.12

and 3.3. So, in the Non-Destructive analysis columns are reported the micro hardness values, previously illustrated in Fig. 6, and the estimated thermal index by using the AIRT setups. As illustrated in Fig. 6, the surface treatment results in an enhancement of the mechanical properties, attributable to microstructural changes. In contrast, the effects of the surface treatment result in a reduction in the thermal properties, as evidenced by a decreasing thermal index in comparison to the untreated material. The validity of these results is further confirmed by the literature, that documented the anticorrelation phenomenon along the depth of the material between local thermal diffusivity and local micro hardness evaluations [34–37]. From the results illustrated in Tables 3, it is evident that an anticorrelation behaviour exists also between mechanical and equivalent thermal properties, properly utilized in this work. On the basis of these considerations, a similar approach can be adopted for the purpose of defining a relation between thermal properties and residual stresses. In fact, an anticorrelation behaviour is established by utilizing the σ_{RS} and the thermal index, which are equivalent parameters capable of accounting for mechanical and thermal behaviours produced by both superficial and in-depth microstructural changes of the material.

In the following part, the definition of the AIRT model for the residual stresses evaluation is detailed.

Fig. 9 shows the analysis carried out to study the main parameters involved during the AIRT tests, necessary for the development of the



Analysis of Variance

Source	DF	Adj SS	Adj MS	F-Value	P-Value
Material	3	35,0540	11,6847	110,02	0,000
Error	6	0,6372	0,1062		
Total	9	35,6912			

Analysis of Variance

Source	DF	Adj SS	Adj MS	F-Value	P-Value
Geometry	2	2,567	1,284	0,27	0,770
Error	7	33,124	4,732		
Total	9	35,691			

Analysis of Variance

Source	DF	Adj SS	Adj MS	F-Value	P-Value
F-Theta lens	1	1,019	1,019	0,24	0,641
Error	8	34,672	4,334		
Total	9	35,691			

Fig. 9. Statistical analysis: (a) material, (b) geometry and (c) F-Theta lens.

AIRT coefficient (n^* see equation (9) in section 2.2). In particular, the analysis was performed by means of individual plot and ANOVA. The estimated thermal index was considered as the response variable during the statistical analysis, while the factors were defined on the basis of the possible parameters involved during the AIRT tests. More in details, the factors considered in the ANOVA were the material (Fig. 9 (a)), the specimen geometries (Fig. 9 (b)) and the presence or absence of the F-Theta lens (Fig. 9 (c)). The material factor (Fig. 9 (a)) included both untreated and treated materials investigated in this study (untreated steels, 20MnCr5-UTM and C45-UTM, treated steels, 20MnCr5-TM and C45-TM). The geometry factor (Fig. 9 (b)) takes into account the possibility of testing gears with different moduli (Gear-M3, gear with 3 mm modulus, Gear-M4, gear with 4 mm modulus) or cylindrical samples (Cyl.Sample). For the F-Theta lens factor (Fig. 9 (c)), the possibility of using two different AIRT setups (with and without the F-Theta lens) was considered in the statistical analysis. Then, the statistically significant association (with 5 % of risk) between the factors and the thermal index was considered for an optimal calibration of the AIRT model. Focusing on the individual plots, a significant variation in the mean of the thermal index responses was observed for the material factor (Fig. 9 (a)). The result was confirmed by the ANOVA analysis (Fig. 9 (a)) as the material factor was statistically significant on the thermal index response with a p-value less than the 0.05 significance level. On the other hand, for the geometry and the F-Theta lens factors (Fig. 9 (b) and 9 (c)), no significant variations in the mean of the thermal indexes were observed. These considerations were confirmed with high p-values in the ANOVA analyses. The results presented in Fig. 9 support the DOE approach, where the laser parameters were appropriately selected to estimate the thermal response only on the basis of the material and independently from tested specimens or the F-Theta lens. For this reason, a proposal of a mathematical formulation based on aspects related to the material was illustrated in equation (9) of Section 2.2, taking into account only Non-Destructive analysis. Moreover, the calibration phase was performed acting on the *ST* coefficient (see equation (9)). On the basis of the obtained results, it was found that an error less than 5 % can be achieved if specific *ST* coefficients are used for each investigated surface treatment. This assumption is justified by the fact that the two investigated surface treatments produced different microstructural changes along the depth of the material, as reported in the metallographic analysis for gears (see the surface treatment patterns of Fig. 7 (a)). So, the *ST* coefficient was chosen equal to 2.7 in case of induction hardening surface treatment, while a value of 2.4 seems to be the most adequate in order to model the carburizing surface treatment.

The results of the proposed AIRT model are now presented.

Fig. 10 illustrates the proposed thermal and mechanical properties modelling described in Section 2.2, starting from the experimental results detailed in Table 3. The blue colours are indicative of the carburizing surface treatment, while the orange colours denote the induction hardening surface treatment. As illustrated in Fig. 10 (a), the linear modelling approach was employed to mathematically describe the Non-Destructive parameters, H and α respectively. The linear modelling presented in Fig. 10 (a) was obtained considering only the Non-Destructive analyses presented in Table 3. In any case, the obtained linear modelling can be considered as representative for each case study, since the results in terms of hardness and thermal index measurements were guaranteed by the high-quality production of all the specimens and by the proposed AIRT methodology. In particular, the hardness uniformity of each specimen was examined through the mechanical characterization (see Fig. 6) confirming the uniformities in terms of production provided by the manufacturer. Then, the AIRT setup allowed for a reliable thermal index measurement (see Table 3) thanks to the optimal laser parameters identified by using the DOE approach. On the other hand, Fig. 10 (b) shows the exponential modelling adopted for the mathematical description of the σ_{RS}. The surface treatment is responsible for the σ_{RS} increment and for the H increment, as consequences of both superficial and in-depth microstructural changes. The mathematical coefficients of both linear (Non-Destructive analysis) and exponential (Destructive analysis) modelling are also illustrated in Fig. 10 for each case study.

Table 4 compares the results obtained from the experimental activity and the AIRT model. In particular, the experimental activity column reports the mathematical coefficients obtained from both linear and exponential modelling by using the experimental data. The slopes (p) were related to the Non-Destructive analysis using the linear modelling

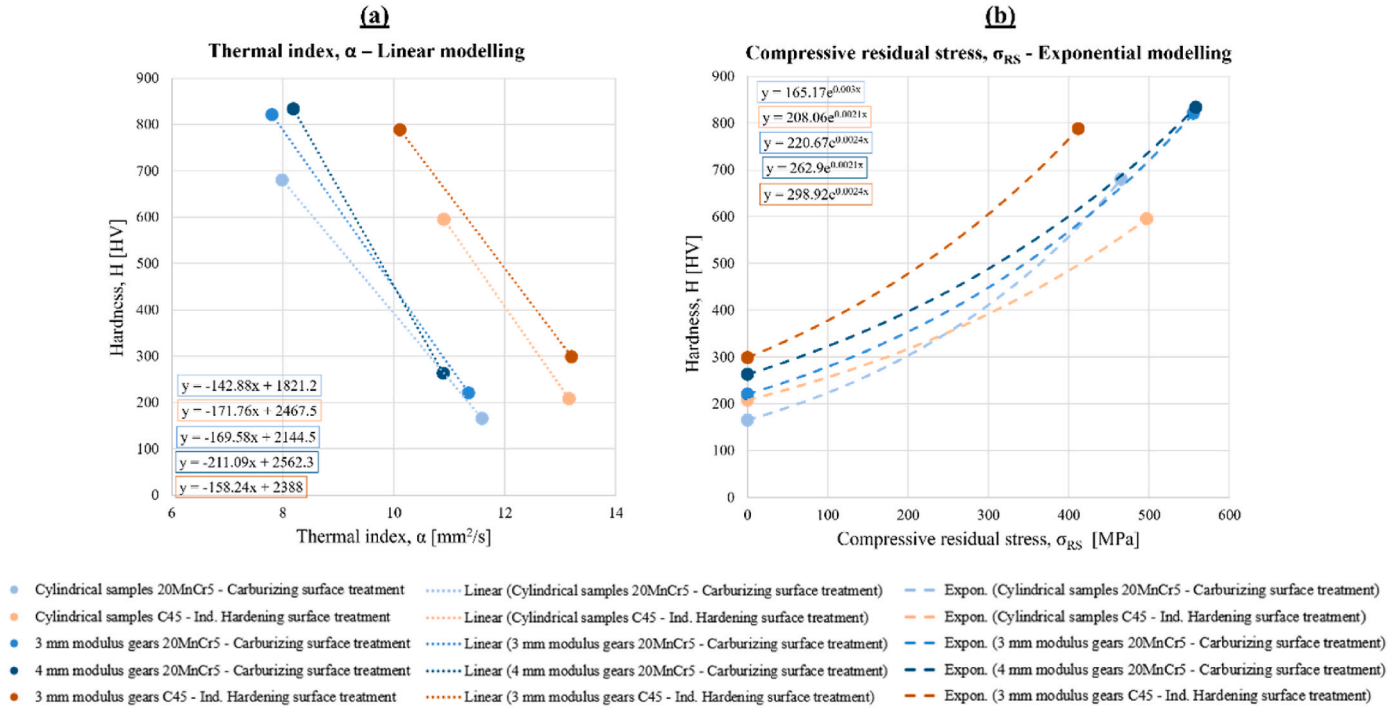


Fig. 10. Thermal and mechanical properties modelling: (a) α, (b) σ_{RS}.

Table 4
Residual stresses analysis.

Case study	Experimental activity		AIRT model		
	Slope, p	*Exponent, n*	*Estimated exponent, n**	*Estimated compressive residual stress, σ_{RS}**	*Error* wrt *X-Ray*
				[MPa]	*[%]*
Cylindrical samples 20MnCr5 - Carburizing surface treatment	−142.88	0.0030	0.0029	485	4.34
Cylindrical samples C45 - Ind. Hardening surface treatment	−171.76	0.0021	0.0022	488	1.9
3 mm modulus gears 20MnCr5 - Carburizing surface treatment	−169.58	0.0024	0.0025	535	3.68
4 mm modulus gears 20MnCr5 - Carburizing surface treatment	−211.09	0.0021	0.0022	585	4.75
3 mm modulus gears C45 - Ind. Hardening surface treatment	−158.24	0.0024	0.0023	414	0.53

(see Fig. 10 (a)), while the exponents (n) were evaluated from the Destructive analysis using the exponential modelling (see Fig. 10 (b)). On the other hand, the AIRT model column reports the results obtained from the proposed Non-Destructive approach. In this case, the residual stresses evaluation was carried out using only Non-Destructive data, H and α respectively. As a matter of fact, the n^* column refers to the estimated AIRT coefficients by using equation (9), in which the slope p and the specific ST coefficient were adopted. Then, the estimated compressive residual stress (σ_{RS}*) with the corresponding error (with respect to the σ_{RS} calculated from the X-Ray diffraction measurements, reported in Fig. 10) is illustrated for each case study. Focusing on the AIRT coefficients, it can be seen that the estimated values (n^*) were comparable to those evaluated experimentally (n), allowing a good approximation of the evolution of the thermal and mechanical properties. The final results (σ_{RS}*) showed that the proposed AIRT model generates an error of less than 5 % when compared with equivalent values obtained from classical apparatus, but with the advantage of a Non-Destructive approach for each specimen that was tested.

The approach presented in this work consists of a new Non-Destructive methodology based on AIRT measurements, which was appropriately calibrated for the evaluation of residual stresses produced in case of surface treatments on mechanical samples and components.

The proposed methodology enhanced the existing literature through the introduction of a new model developed using a similarity to coatings concept, which exploits the idea of equivalent thermal diffusivity. The model was formulated on the basis of Lock-In Thermography and hardness measurements, with the objective of taking into account the microstructural changes produced by the surface treatment. This methodology enabled the evaluation of residual stress considering exclusively Non-Destructive measurements, even in cases of complex mechanical components such as gears.

5. Conclusions

This work presents an AIRT-based Non-Destructive approach for the evaluation of residual stresses generated by surface treatments. A series of case studies involving cylindrical samples and gears with varying geometries, in combination with two different surface treatments, were investigated. The obtained results allowed the following conclusions to be drawn.

The DOE activity was adopted for the evaluation of the laser parameters, and the tuning was performed for the untreated materials since it is easy to thermally characterize. Then, the same amount of energy, if provided to the treated material, allowed to quantify the thermal properties reduction as a consequence of the surface treatment.

The AIRT model, developed using a similarity to coatings concept, exploits the advantages of an anticorrelation phenomenon with equivalent mechanical and thermal properties. The thermal diffusivity becomes the AIRT thermal index for a Non-Destructive residual stresses evaluation. The results obtained during the AIRT model definition (individual plots and ANOVA analysis) confirm the approach developed during the DOE. As a matter of fact, possible effects of the experimental setup were properly considered during the laser parameters tuning, leaving the thermal indexes variation only to the microstructural changes. Furthermore, the impact of the hardening pattern produced from each surface treatment was considered with the ST coefficient.

In any case, the proposed Non-Destructive approach allowed for a satisfactory evaluation of the compressive residual stresses for each case study, and the results were confirmed by those obtained from X-Ray measurements (errors less than 5 %). Moreover, the residual stresses evaluation was performed considering only Non-Destructive measurements, the thermal index and the superficial micro hardness of the tested zones. At the end, the utilization of an AIRT configuration offers notable advantages, particularly in the evaluation of thermal properties for complex mechanical components, such as gears, where the employment of conventional apparatus, such as the Hot-Disk, is not applicable.

CRediT authorship contribution statement

Luca Corsaro: Writing – original draft, Validation, Conceptualization. **Francesca Curà:** Project administration, Methodology, Funding acquisition. **Raffaella Sesana:** Supervision, Methodology, Data curation.

Declaration of competing interest

The authors declare that they have no known competing financial interests or personal relationships that could have appeared to influence the work reported in this paper.

Acknowledgements

This work was supported by Proof Of Concept project “Sviluppo e set up di una metodologia basata sulla termografia attiva per la misura delle tensioni residue nei materiali e nei componenti metallici”. Acknowledgments are attributed to Compagnia di San Paolo for its financial support.

Data availability

Data will be made available on request.

References

[1] Totten GE, Maurice AHH, Tatsuo I. Handbook of residual stress and deformation of steel. first ed. Materials Park, OH: ASM International; 2002.
[2] Rossini NS, Dassisti M, Benyounis KY, Olabi AG. Methods of measuring residual stresses in components. Mater Des 2012;35:572–88.

[3] Otsuki A. Non-Destructive material characterization methods. first ed. Amsterdam: Elsevier; 2024.
[4] Arnold W, Goebbels K, Kumar A. Non-destructive materials characterization and evaluation. first ed. Berlin Heidelberg: Springer; 2023.
[5] Gou R, Zhang Y, Xu X, Sun L, Yang Y. Residual stress measurement of new and in-service X70 pipelines by X-ray diffraction method. NDT E Int 2011;44(5):387–93. https://doi.org/10.1016/j.ndteint.2011.03.003.
[6] Pierret S, Evans A, Paradowska AM, Kaestner A, James J, Etter T, et al. Combining neutron diffraction and imaging for residual strain measurements in a single crystal turbine blade. NDT E Int 2012;45(1):39–45. https://doi.org/10.1016/j.ndteint.2011.08.009.
[7] Rego R, Löpenhaus C, Gomes J, Klocke F. Residual stress interaction on gear manufacturing. J Mater Process Technol 2018;252:249–58. https://doi.org/10.1016/j.jmatprotec.2017.09.017.
[8] Savaria V, Monajati H, Bridier F, Bocher P. Measurement and correction of residual stress gradients in aeronautical gears after various induction surface hardening treatments. J Mater Process Technol 2015;220:113–23. https://doi.org/10.1016/j.jmatprotec.2014.12.009.
[9] Sorsa A, Leiviskä K, Santa-aho S, Lepistö T. Quantitative prediction of residual stress and hardness in case-hardened steel based on the Barkhausen noise measurement. NDT E Int 2012;46:100–6. https://doi.org/10.1016/j.ndteint.2011.11.008.
[10] Desvaux S, Duquennoy M, Gualandri J, Ourak M. The evaluation of surface residual stress in aeronautic bearings using the Barkhausen noise effect. NDT E Int 2004;37(1):9–17. https://doi.org/10.1016/S0963-8695(03)00046-X.
[11] Zhang Y, Hu D, Chen J, Yin L. Research on non-destructive testing of stress in ferromagnetic components based on metal magnetic memory and the Barkhausen effect. NDT E Int 2023;138:102881. https://doi.org/10.1016/j.ndteint.2023.102881.
[12] Jaramillo J, Sánchez JC, Suárez-Bustamante FA, Vargas D, Vargas G, Toro A, Franco FA. Implementation of the magnetic barkhausen noise technique for microstructural characterization of rail steel. NDT E Int 2025;44(2). https://doi.org/10.1007/s10921-025-01184-y.
[13] Lee JH, Park KY, Joh C, Choi JY, Kwahk I. Measuring stress of strand using magnetic barkhausen noise measured by solenoid-type sensor. NDT E Int 2025;40(4):1592–609. https://doi.org/10.1080/10589759.2024.2346775.
[14] Pritchard SE. The use of ultrasonics for residual stress analysis. NDT E Int 1987;20(1):57–60. https://doi.org/10.1016/0308-9126(87)90373-7.
[15] Jiao J, Li L, Zhang H, Lv H, Wu B, He C. Ultrasonic immersion testing of residual stress in plates using collinear Lamb wave mixing technique. NDT E Int 2024;146:103153. https://doi.org/10.1016/j.ndteint.2024.103153.
[16] Ono K. Residual stress determination using magnetomechanical acoustic emission. NDT E Int 1996;29(5):346. https://doi.org/10.1016/S0963-8695(97)81607-6.
[17] Zhang Y, Xue H, Yang Y, Wang S, Wang Z, Wu J, Yang C. Nondestructive testing method of residual stresses in metallic materials based on Knoop indentation technique. NDT E Int 2025;40(1):188–205. https://doi.org/10.1080/10589759.2024.2315210.
[18] Li L, Li H, Yang S, Wang Z. Evaluation of equibiaxial residual stress in metal materials using indentation testing techniques. Mater Today Commun 2025;42:111268. https://doi.org/10.1016/j.mtcomm.2024.111268.
[19] Peng L, Benavidez E, Mukherjee S, Morales RE, Tringe JW, Stobbe D, Deng Y. In-situ 3D temperature field modeling and characterization using eddy current for metal additive manufacturing process monitoring. Sci Rep 2025;15(1):9999. https://doi.org/10.1038/s41598-025-94553-6. 15.
[20] Rodríguez VM, Nadimpalli VK, Pedersen DB, Ruiz A. Nondestructive evaluation of tempering treatment in a spray-formed 440C martensitic stainless steel using thermoelectric power measurements. MRS Advances 2025;10(1):108–14. https://doi.org/10.1557/s43580-024-01060-3.
[21] Kang K, Du Y, Wang S, Li L, Wang Z, Li C. Full-field stress measuring method based on terahertz time-domain spectroscopy. Opt Express 2021;29(24):40205–13. https://doi.org/10.1364/OE.435386.
[22] Lin H, Shi T, Huang Y, Zhong S, Wang B, Zhang Z, Huang Y. Measurement of stress optical coefficients for GFRP based on terahertz time-domain spectroscopy. Opt Mater 2024;157:116281. https://doi.org/10.1016/j.optmat.2024.116281.
[23] Maldague XPV. Nondestructive evaluation of materials by infrared thermography. first ed. London: Springer; 1993.
[24] Ibarra-Castanedo C, Piau JM, Guilbert S, Avdelidis NP, Genest M, Bendada A, Maldague XPV. Comparative study of active thermography techniques for the nondestructive evaluation of honeycomb structures. Res Nondestr Eval 2009;20(1):1–31. https://doi.org/10.1080/09349840802366617.
[25] Halloua H, Obbadi A, Errami Y, Sahnoun S, Elhassnaoui A. Nondestructive inverse approach for determining thermal and geometrical properties of internal defects in CFRP composites by lock-in thermography. In: International conference on electrical sciences and technologies in maghreb (CISTEM); 2016. p. 1–7. https://doi.org/10.1109/CISTEM.2016.8066828.
[26] Dattoma V, Marcuccio R, Pappalettere C, Smith GM. Thermographic investigation of sandwich structure made of composite material. NDT E Int 2001;34(8):515–20. https://doi.org/10.1016/S0963-8695(00)00082-7.
[27] Xie J, Chen L, Han Y, Huang W, Li G, Xu C. Visualization of hidden cracks under corrosion layer in steel structures via eddy current pulsed thermography: simulation and experiment. NDT E Int 2025;152:103321. https://doi.org/10.1016/j.ndteint.2025.103321.
[28] Hwang S, An YK, Kim JM, Sohn H. Monitoring and instantaneous evaluation of fatigue crack using integrated passive and active laser thermography. Opt Laser Eng 2019;119:9–17. https://doi.org/10.1016/j.optlaseng.2019.02.001.
[29] Curà F, Sesana R, Corsaro L, Mantoan R. Characterization of thermal barrier coatings using an active thermography approach. Ceramics 2022;5(4):848–61. https://doi.org/10.3390/ceramics5040062.
[30] Huang Z, Zhu J, Zhuo L, Li C, Liu C, Hao W, Xie W. Non-destructive evaluation of uneven coating thickness based on active long pulse thermography. NDT E Int 2022;130:102672. https://doi.org/10.1016/j.ndteint.2022.102672.
[31] Li Y, Yang Z, Zhu J, Ming A, Zhang W, Zhang J. Investigation on the damage evolution in the impacted composite material based on active infrared thermography. NDT E Int 2016;83:114–22. https://doi.org/10.1016/j.ndteint.2016.06.008.
[32] Sesana R, Corsaro L, Cura FM. Active thermography technique for fatigue damage characterization in gears. In: 20th International Conference on Experimental Mechanics, 10; 2023. p. 1069–76.
[33] Dell'Avvocato G, Palumbo D, Galietti U. A non-destructive thermographic procedure for the evaluation of heat treatment in Usibor®1500 through the thermal diffusivity measurement. NDT E Int 2023;133:102748. https://doi.org/10.1016/j.ndteint.2022.102748.
[34] Liu Y, Baddour N, Mandelis A, Beingessner C. Photothermal depth profilometry of heat-treated hardened 0.15%–0.2%C, 0.6%–0.9%Mn Steels. J Appl Phys 2004;96(3):1521–8. https://doi.org/10.1063/1.1765868.
[35] Nicolaides L, Mandelis A, Beingessner CJ. Physical mechanisms of thermal-diffusivity depth-profile generation in a hardened low-alloy Mn, Si, Cr, Mo steel reconstructed by photothermal radiometry. J Appl Phys 2001;89(12):7879–84. https://doi.org/10.1063/1.1373698.
[36] Wang C, Mandelis A. Evaluation of effective case depth in heat treated steel products using photothermal radiometry. European Phys J 2008;153(1):373–6. https://doi.org/10.1140/epjst/e2008-00465-9.
[37] Wang C, Mandelis A. Evaluation of effective case depth in heat treated steel products using photothermal radiometry. European Phys J 2008;153(1):373–6. https://doi.org/10.1140/epjst/e2008-00465-9.
[38] Guo X, Sivagurunathan K, Garcia J, Mandelis A, Giunta S, Milletari S. Laser photothermal radiometric instrumentation for fast in-line industrial steel hardness inspection and case depth measurements. Appl Optics. Optical Tech Biomed Optics. 2009;48(7):C11. https://doi.org/10.1364/AO.48.000C11.
[39] Velazquez-Hernandez R, Melnikov A, Mandelis A, Sivagurunathan K, Rodriguez-Garcia ME, Garcia J. Non-destructive measurements of large case depths in hardened steels using the thermal-wave radar. NDT E Int 2012;45(1):16–21. https://doi.org/10.1016/j.ndteint.2011.08.006.
[40] Zhu P, Wang R, Sivagurunathan K, Sfarra S, Sarasini F, Ibarra-Castanedo C, Maldague X, Zhang H, Mandelis A. Frequency multiplexed photothermal correlation tomography for non-destructive evaluation of manufactured materials. Int J Extrem Manuf 2025;7(3):35601. https://doi.org/10.1088/2631-7990/ada837.
[41] Zhu P, Wang R, Sfarra S, Vavilov V, Maldague X, Zhang H. A novel force-temperature model for evaluating internal forces in CFRP by means of infrared thermography. NDT E Int 2024;143:103066. https://doi.org/10.1016/j.ndteint.2024.103066.
[42] Zhu P, Zhang H, Santulli C, Sfarra S, Maldague X. Evaluation of residual stress in modified and pure HDPE materials based on thermal diffusivity and terahertz phase spectroscopy. Eng Proceed 2023;51(1):33. https://doi.org/10.3390/engproc2023051033.
[43] Zhu P, Zhang H, Santulli C, Sfarra S, Usamentiaga R, Vavilov VP, Maldague X. Contactless and nondestructive evaluation of residual stress distribution in modified and pure HDPE materials using a novel terahertz method and line-scan thermographic technique. Composites. Part A. Appl Sci Manufact 2024;183:108220. https://doi.org/10.1016/j.compositesa.2024.108220.
[44] ISO 18555. Metallic and other inorganic coatings. Determination of thermal conductivity of thermal barrier coatings. 2016.
[45] ISO 18755. Fine ceramics (advanced ceramics, advanced technical ceramics). Determination of thermal diffusivity of monolithic ceramics by flash method. 2022.
[46] Salazar A, Colom M, Mendioroz A. Laser-spot step-heating thermography to measure the thermal diffusivity of solids. Int J Therm Sci 2021;170:107124. https://doi.org/10.1016/j.ijthermalsci.2021.107124.
[47] ISO 6336. Calculation of load capacity of spur and helical gears. Part 3: calculation of tooth bending strength. 2019.
[48] ISO 6336. Calculation of load capacity of spur and helical gears. Part 5: Strength Qualiy of Materials 2016.
[49] Curà F, Sesana R, Corsaro L, Santoro L. Metodo di rilevazione delle tensioni residue su materiali e componenti mediante tecniche di termografia attiva. Patent application for industrial invention n. 102023000003597. 2023.
[50] Curà F, Corsaro L, Tromba L. Lock-in thermography for surface treatment characterization in gears. Eng Proceed 2025;85(1):2.
[51] Corsaro L, Curà F, Sesana R. Active thermography for residual stresses identification in gears. In: International symposium on industrial engineering and automation. Springer Nature Switzerland; 2024. p. 116–25.
[52] Taguchi designs. Minitab. https://support.minitab.com/en-us/minitab/help-and-how-to/statistical-modeling/doe/supporting-topics/taguchi-designs/taguchi-designs/.
[53] What is a response surface design. Minitab. https://support.minitab.com/en-us/minitab/help-and-how-to/statistical-modeling/doe/supporting-topics/response-surface-designs/response-surface-central-composite-and-box-behnken-designs/#what-is-a-response-surface-design.